

Retrieval-guided Cross-view Image Synthesis

Hongji Yang *

Yiru Li*

2070276033@email.szu.edu.cn

2350271010@email.szu.edu.cn

Shenzhen University

Shenzhen, China

Yingying Zhu

zhuyy@szu.edu.cn

Shenzhen University

Shenzhen, China

Abstract

Information retrieval techniques have demonstrated exceptional capabilities in identifying semantic similarities across diverse domains through robust feature representations. However, their potential in guiding synthesis tasks, particularly cross-view image synthesis, remains underexplored. Cross-view image synthesis presents significant challenges in establishing reliable correspondences between drastically different viewpoints. To address this, we propose a novel retrieval-guided framework that reimagines how retrieval techniques can facilitate effective cross-view image synthesis. Unlike existing methods that rely on auxiliary information, such as semantic segmentation maps or preprocessing modules, our retrieval-guided framework captures semantic similarities across different viewpoints, trained through contrastive learning to create a smooth embedding space. Furthermore, a novel fusion mechanism leverages these embeddings to guide image synthesis while learning and encoding both view-invariant and view-specific features. To further advance this area, we introduce VIGOR-GEN, a new urban-focused dataset with complex viewpoint variations in real-world scenarios. Extensive experiments demonstrate that our retrieval-guided approach significantly outperforms existing methods on the CVUSA, CVACT and VIGOR-GEN datasets, particularly in retrieval accuracy (R@1) and synthesis quality (FID). Our work bridges information retrieval and synthesis tasks, offering insights into how retrieval techniques can address complex cross-domain synthesis challenges.

CCS Concepts

• **Computing methodologies** → **Visual content-based indexing and retrieval.**

Keywords

Semantic similarity, Cross-view image synthesis, Retrieval-guided, Viewpoints differences

1 Introduction

While information retrieval techniques have shown remarkable success in various domains, their potential in guiding image synthesis remains largely unexplored. In this paper, we investigate how retrieval mechanisms can be leveraged to address a fundamental challenge in cross-view image synthesis: bridging the significant domain gap between different viewpoints. We demonstrate how advances in retrieval techniques can go beyond traditional retrieval scenarios, offering valuable insights for addressing complex cross-domain visual tasks through semantic similarity modeling.

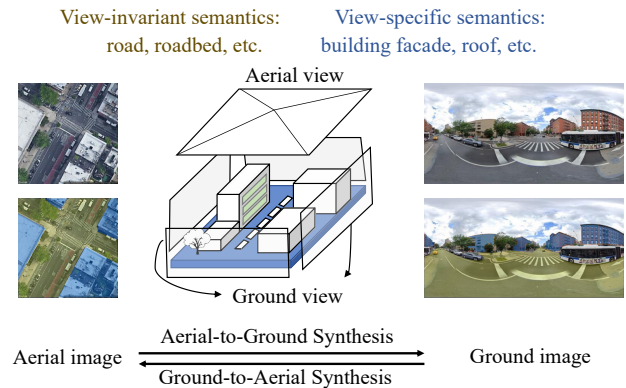


Figure 1: Illustrating view-invariant and view-specific semantics in cross-view image synthesis between aerial and ground views.

Cross-view image synthesis aims to generate an image from a novel viewpoint, given one input image from different viewpoint, such as transforming an aerial (bird’s-eye) view into a ground (street) view. [8, 23, 28, 30, 32, 35]. This technique can benefit a wide range of applications, from autonomous driving and robot navigation to 3D reconstruction [16], virtual/augmented reality [1], and urban planning [18].

While promising, existing cross-view image synthesis methods often rely on auxiliary information, such as semantic segmentation maps [23, 30, 35], or employ preprocessing modules like polar-transformation [15, 28, 32] to bridge the domain gap between different views. These additional requirements not only introduce significant computational overhead but also complicate the synthesis process, particularly in reverse generation scenarios (e.g., ground-to-aerial synthesis). The reliance on such auxiliary components fails to effectively address a critical challenge in cross-view synthesis - establishing reliable correspondences between drastically different viewpoints, where visual appearances exhibit significant variations. As shown in Figure 1’s lower half, view-specific semantics (highlighted in translucent blue) represent objects with drastically different appearances across viewpoints, exemplified by a building’s roof in aerial view versus its facade in ground view. View-specific semantics not only play an important role in establishing reliable correspondences between different viewpoints, but also provide clues to the fidelity and realism of the synthesized images. In contrast to view-specific semantics, view-invariant semantics (highlighted in translucent yellowish-green) represent elements that preserve their essential characteristics across different viewpoints - for example, while roads may appear visually different

*Both authors contributed equally to this research.

from aerial and ground views, their basic layout remain consistent, enabling reliable cross-view correspondence. We observe that these challenges parallel key problems in information retrieval, particularly in capturing semantic similarities despite visual differences. This parallel suggests that retrieval techniques could offer valuable insights for addressing cross-view synthesis challenges.

Moreover, existing datasets for cross-view image synthesis primarily focus on rural and suburban areas, overlooking the complexities of urban environments. This lack of diversity in training data makes it challenging to develop models that can effectively synthesize images in more realistic and challenging scenarios.

Inspired by the inherent capability of retrieval tasks to measure semantic similarity, we leverage a retrieval network as an embedder to encode these semantics and guide the generation process, eliminating the need for additional annotations or preprocessing steps. The novel retrieval-guided cross-view image synthesis method that does not require semantic segmentation maps or preprocessing modules while generating high-fidelity, realistic target-view images by fully leveraging view-invariant and view-specific semantics. To enhance image quality and realism, our method incorporates view-specific semantics by adopting noise and a modulated style to diversify visual features. We fuse retrieval embedding and style at various layers to improve consistency and image quality. Additionally, to address the scarcity of urban datasets for cross-view image synthesis, we introduce VIGOR-GEN, a derived urban dataset. We validate our proposed method through comprehensive experiments on CVUSA [37], CVACT [14], and the more challenging VIGOR-GEN dataset. Our retrieval-guided model generates more realistic images and significantly outperforms state-of-the-art methods, particularly in terms of SSIM and FID. Extensive ablation studies corroborate the efficacy of each component in our method.

The main contributions of our work are summarized as follows:

- Introduction of Retrieval Techniques in Cross-view Image Synthesis.** Since retrieval networks have traditionally excelled at measuring semantic similarity, we demonstrate their potential as a powerful guiding mechanism for generative tasks. This dual application of retrieval techniques opens up new possibilities for the retrieval and synthesis research communities.
- Retrieval-guided Framework for Bridging Domain Gap.** We introduce a retrieval-guided framework that leverages a retrieval network as an embedder. This network is trained to measure the similarity of view-invariant features between different views, effectively bridging the domain gap without needing semantic segmentation maps or preprocessing modules. Our model simplifies the synthesis process and makes reverse generation more straightforward.
- Novel Generator for Enhanced Semantic Consistency and Diversity.** Our method includes a new generator that incorporates both retrieval embedding and style information at various layers. This approach improves the correspondence between views by leveraging view-invariant semantics captured by the retrieval network while also enhancing the diversity and realism of view-specific semantics using noise and modulated style techniques. This leads to synthesized images with higher fidelity and a more natural appearance.
- New Dataset for Urban Environments (VIGOR-GEN).** We build a new derived dataset called VIGOR-GEN, which provides a more challenging and realistic setting for training and evaluating cross-view image synthesis models, pushing the boundaries of the field beyond existing rural and suburban datasets. Our method demonstrates superior performance in synthesizing photo-realistic images from a single input image in another view, as evidenced by its performance on well-known datasets and the new VIGOR-GEN dataset.

2 Related Work

Semantic-guided Cross-view Synthesis. The first pipeline is to apply the semantic segmentation maps of the target-view images to guide the generative model. Zhai [37] proposed a linear transformation module to generate a panorama through supervised information from a transformed semantic layout of aerial images. Regmi and Borji [23] designed two cGAN models, X-fork and X-seq, for simultaneously predicting the target image and the semantic map. Tang [30] regarded cross-view image synthesis as an image-to-image translation task. This work applied the semantic map of the target view and the source view image as inputs and then obtained the predicted target images. To generate 360-degree panorama images, Wu [35] proposed PanoGAN as well as a new discrimination mechanism. Zhu [45] proposed a Parallel Progressive GAN to stabilize the training of cross-view image synthesis and thus generated rich details.

Preprocessing-guided Cross-view Synthesis. Another pipeline involves a preprocessing module to assimilate the source view image into the target view image. Lu [15] proposed a projection transformation module that is trained by height and semantic information estimated from aerial images. However, this approach requires ground-truth height supervision for the dataset and carries a complicated pipeline. Toker [32] first applied the polar transformation proposed by Shi [29] to cross-view image synthesis, which greatly reduces the domain gap between two views. Besides, Toker [32] proposed a new multi-tasks framework Coming-Down-to-Earth (CDE) for synthesis, where they postulated that retrieval and synthesis tasks are orthogonal. This approach further improves the correspondence of generation but fails to produce better image detail and quality. Shi [28] proposed an end-to-end network that employs a learnable geographic projection module to learn the projection relationship from the aerial view to the ground view, and then feed the manipulated image into the later generator.

As a striking difference from existing works, without the help of semantic maps and preprocessing, our model can synthesize a more realistic target-view image and retain rich details, capable of realizing the mutual generation of ground panorama and aerial image.

Generative Model. In recent years, diffusion model [4, 22, 25, 26] achieved great success, which produces higher quality images at the cost of a large amount of resources. In addition, there are still neglected problems in cross-view image synthesis, as described in the next section. Moreover, earlier work on cross-view generation does not yield better performance with more artifacts. Therefore, it

is essential to study a competitive GAN model before moving fully towards the diffusion model.

3 Methodology

3.1 Overview of Retrieval-Guided Framework

Inspired by advances in information retrieval, we propose a novel cross-view image synthesis framework that leverages a pre-trained and fixed retrieval model to identify view-invariant semantics and view-invariant semantics, enabling an end-to-end program without requiring preprocessing or additional input.

The embedder, trained through contrastive learning, maps view-invariant semantics into a continuous space, allowing for fusion in the deeper layers. This approach aims to extract embeddings that minimize visual differences, ensuring a smooth transformation of view-invariant semantics from the source domain to the target domain via the generator, thereby preserving the image structure.

Moreover, the embedding can also serve as the condition in the discriminator to guide the generator to improve correspondence. Meanwhile, we consider the ability of the model to generate view-specific semantics in the target domain by offering modulated style information. Although it is difficult to generate identical target-view images, our goal is to ensure that the retrieval-driven view-invariant semantics in the generated images are consistent between the two views while the view-specific semantics remain as visually reasonable as possible.

3.2 Network Architecture

The overall architecture of our network is illustrated in Figure 2. It consists of two components: the mapping network and the retrieval network. **The Mapping Network:** our network has a mapping network which has already been shown in several works [3, 9–11]. The mapping network learns how to transform the noise sampled from a Gaussian distribution to a new style distribution to better generate view-specific semantics representations, thus yielding detail-enriched images. This transformation also enhances the quality of image features for retrieval tasks. It consists of four fully connected layers with non-linearity, producing discriminative features useful for retrieval. **The Retrieval Network:** we adopt the retrieval network proposed in [46] because of its simplicity and effectiveness. It owns stacked attention layers for better feature extraction and encoding for retrieval. The attention mechanism aligns different views, embedding images into a common space for efficient retrieval. We utilize its shallower version SAIG-S [46] here. This retrieval network can settle visual differences and directly embed images from different views into a smooth space.

3.3 Structure & Facade Generation

Two-stage generation. In general, the generative model controls the generation of structures at low resolutions ($\leq 32 \times 32$), while features such as facade and color will be affected in higher resolutions ($\geq 32 \times 32$) [11, 24, 36]. This hierarchical generation process is highly relevant to information retrieval, as low-resolution structures are first generated and then refined, facilitating a smooth transition in visual features for better matching during retrieval. Therefore, we refine the goals of the generator: at low resolution, the generator focuses on projecting the view-invariant semantics

into target-view space. Once the approximate structure of the target view has been generated, the generator then turns its attention to how to generate facades while preserving identity.

Attentional AdaIN. The embedding extracted by the retrieval model contains the semantic information of the location. Some work [5, 7, 20, 31, 43] has explored how to incorporate the latent code into feature maps to acquire target images. In the context of image retrieval, this latent code helps in transferring the identity and semantic features learned during retrieval directly into the generative process, ensuring that the generated images align with the target view while preserving relevant semantic details. To better inject identity information into the image, we perform some changes to AdaIN [7] to make feature maps more semantically consistent with the given source image. Given an input $\mathbb{X} \in \mathbb{R}^{n \times c \times h \times w}$, we first normalize it into zero mean and unit deviation:

$$\hat{\mathbb{X}} = \frac{\mathbb{X} - \mu_{nc}}{\sigma_{nc}}, \mu_{nc} = \frac{1}{hw} \sum_{hw} \mathbb{X}, \sigma_{nc} = \sqrt{\frac{1}{hw} \sum_{hw} (\mathbb{X} - \mu_{nc}^2) + \epsilon} \quad (1)$$

where ϵ is a small constant to prevent the divisor from being zero, μ_{nc} denotes the mean and σ_{nc} denotes the variance.

Subsequently, the modulation parameters γ and β are learned by MLP from the retrieval feature \tilde{r} :

$$\gamma_r = MLP_{\gamma}(\tilde{r}), \beta_r = MLP_{\beta}(\tilde{r}) \quad (2)$$

Then, the denormalization can be realized as follows:

$$\hat{\mathbb{X}}_r = \gamma_r \hat{\mathbb{X}} + \beta_r \quad (3)$$

To decide which region and to what extent it can reinforce the retrieval embedding on the image feature, we utilize input \mathbb{X} to learn to obtain a weight map M . It can be described as:

$$M = Sigmoid(Cono(\hat{\mathbb{X}})) \quad (4)$$

where *Sigmoid* denotes the sigmoid activate function. In the ideal case, we expect the modulation of retrieval embeddings to work on the areas where the source view is relevant to the target view.

Finally, the feature maps are summed by M on the pixel-wise level:

$$\hat{\mathbb{X}} = \hat{\mathbb{X}}_r \cdot M + \hat{\mathbb{X}} \cdot (1 - M) \quad (5)$$

Different residual modules. Residual structures have been widely applied in prior work [23, 28, 30, 35, 45] on cross-view image synthesis to aid in structure generation. However, other work [10, 11] argues that residual structures introduce varying degrees of artifacts and blurring in generation, especially in facade generation. Therefore, the modules for generating structures and facades have to be carefully considered, according to different task objectives.

For structure generation, we use a residual structure similar to previous methods, except for the use of an improved AdaIN in the normalization layer. Both the principal and residual paths are injected with retrieval embedding to facilitate the construction of the structure. For facade generation, we follow the network design of previous work [10, 11], but the residual structure is also used. The input latent is first fed into AdaIN and the convolution layer to fuse the modulated style. The residual structure is designed to be set after the convolution layer and continue to fuse the embedding

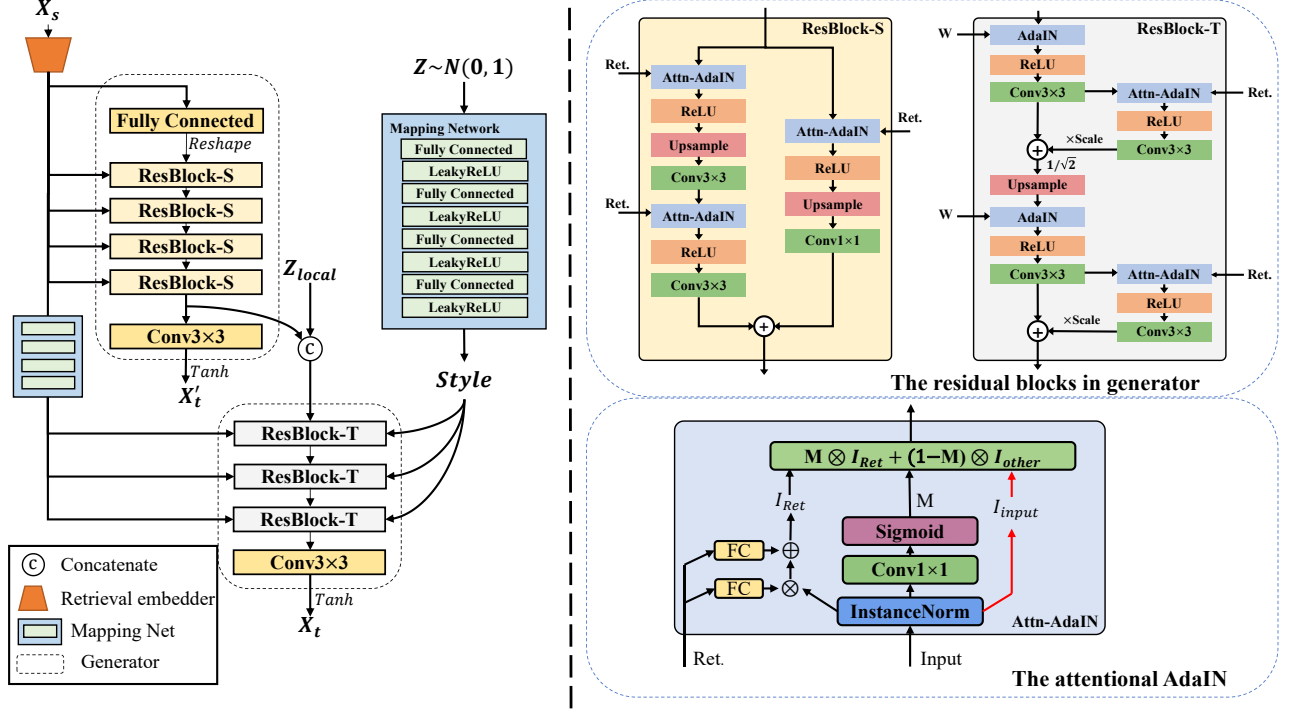


Figure 2: Illustration of our network architecture. left: our network consists of a structure generator, a facade generator, a mapping network, and a retrieval embedder. right-top: the residual blocks in our generator. right-bottom: the attentional AdaIN in different residual blocks.

through an improved AdaIN. The residual path is then multiplied by a layer scale [27, 33] to perform gradual fading.

Generator. As shown in Figure 2, our generator first gains the retrieval embedding from the source images \mathbb{X}_s as the input, which is then integrated into a fully connected layer and is reshaped to be equally proportional to the target image \mathbb{X}_t in length and width. The latent feature synthesized by the structure generator is then concatenated with a noise vector sampled from the Gaussian distribution. The generator gradually increases the scale of the feature map and eventually converts it into an image. Each residual block in the decoder contains 1) Normalization layers integrating style information or retrieval information; 2) Convolutional layers with spectral normalization [19] and 3) Activate function.

Discriminator. To guide our generator to synthesize more realistic and semantically consistent images with the source image, we adopt the idea of a one-way discriminator proposed in [31]. It first extracts the features of the synthesized image and then concatenates them with the spatially extended embedding vector. The discriminator should assign the realistic and matching images with high scores, and the fake or mismatched images with low scores.

3.4 Loss Function

Discriminator Loss. Since the one-way discriminator is employed, we apply the same adversarial loss [31] except for the gradient penalty to train our network.

$$\begin{aligned} \mathcal{L}_{adv}^D = & -\mathbb{E}_{\mathbb{X} \sim \mathbb{P}_r} [\min(0, -1 + D(\mathbb{X}, \tilde{\mathbb{A}}))] \\ & - (1/2)\mathbb{E}_{\tilde{\mathbb{X}} \sim \mathbb{P}_g} [\min(0, -1 - D(\tilde{\mathbb{X}}, \tilde{\mathbb{A}}))] \\ & - (1/2)\mathbb{E}_{\mathbb{X} \sim \mathbb{P}_{mis}} [\min(0, -1 - D(\mathbb{X}, \tilde{\mathbb{A}}))] \end{aligned} \quad (6)$$

where $\tilde{\mathbb{A}}$ refers to the retrieval embeddings of the real image \mathbb{X} and $\tilde{\mathbb{X}}$ denotes the synthesized image.

Generator Loss. The reconstruction loss is employed to ensure that the target \mathbb{X}_t is equivalent to the final result \mathbb{X}_r on a pixel-wise level. It can be defined as follows:

$$\mathcal{L}_{rec} = \|\mathbb{X}_t - \mathbb{X}_r\|^1 \quad (7)$$

To further improve the realism, we follow the Learned Perceptual Image Patch Similarity (LPIPS) [40] loss. Thus, the perceptual loss is defined as:

$$\mathcal{L}_{perc} = \|\phi(\mathbb{X}_t) - \phi(\mathbb{X}_r)\|^1 \quad (8)$$

where ϕ denotes the pre-trained VGG network.

To ensure that the synthesized image has the same view-invariant semantics information as the target image, we use identity loss, which is defined as:

$$\begin{aligned} \mathcal{L}_{id} = & 1 - \cos(R(\mathbb{X}_r), R(\mathbb{X}_t)) \\ & + 1 - \cos(R(\mathbb{X}'_r), R(\mathbb{X}'_t)) \end{aligned} \quad (9)$$

where $\cos(\cdot, \cdot)$ denotes the cosine similarity between the output embedding vectors and \mathbb{X}'_r means the low-resolution generated image. R denotes the pre-trained retrieval network as in Sec. 3.2.

To prevent the model from generating repetitive content, we apply a diversity loss [13, 17] between a pair of local code Z_{local} . The diversity loss is defined as:

$$\mathcal{L}_{div} = \frac{d_z(z_{local_1}, z_{local_2})}{d_I(G(w, z_{local_1}, \tilde{\mathbf{A}}), G(w, z_{local_2}, \tilde{\mathbf{A}}))} \quad (10)$$

where $d_z(\cdot, \cdot)$ and $d_I(\cdot, \cdot)$ denote the $L1$ distance between the latent codes or images, G is the generator.

The adversarial loss of the generator is as follows:

$$\mathcal{L}_{adv}^G = \mathbb{E}_{\hat{x} \sim \mathbb{P}_g} [D(\hat{x}, \tilde{\mathbf{A}})] \quad (11)$$

The total loss for the generator is a weighted sum of the above losses, formulated as:

$$\mathcal{L}_G = \mathcal{L}_{adv}^G + \lambda_{rec} \mathcal{L}_{rec} + \lambda_{perc} \mathcal{L}_{perc} + \lambda_{id} \mathcal{L}_{id} + \lambda_{div} \mathcal{L}_{div} \quad (12)$$

4 VIGOR-GEN Dataset

For cross-view image synthesis, the commonly used CVUSA [37] and CVACT [14] datasets are primarily field and sub-urban images with an open field of view and less occlusion. The buildings on both datasets are mostly cottages or bungalows, with simple facade information. In contrast to the above datasets, the images with soaring skyscrapers in urban areas often have narrower views and more occlusions, while the complex street surroundings and building facades raise greater challenges to generative networks. To fit realistic scenarios, the cross-view image synthesis generates the need for an urban area dataset. To this end, we have collected a derived dataset of cross-view urban images, VIGOR-GEN, consisting of 103,516 image pairs.

All images are collected from Google Map API. The dataset is mainly extended on cross-view image retrieval dataset VIGOR [44]. To ensure that images synthesized across different views have the same identity as the source image, this task usually requires center-aligned image pairs to avoid ambiguities, so the original VIGOR urban dataset (which is set to be non-centrally aligned) cannot be directly applied to this task. To extend the application of this dataset, we present a derived dataset in this work so that it can be used for cross-view image synthesis. Table 1 shows the comparison of different datasets.

5 Experiment

5.1 Implementation Details

Datasets. We conducted on three panorama-aerial dataset: CVUSA [38], CVACT [14] and our proposed VIGOR-GEN datasets. Following [28, 32], CVACT [14] and CVUSA [38] contain 35,532 satellite and street-view image pairs for training and 8,884 image pairs for testing. The VIGOR-GEN dataset comprises 51,366 images for training and 51,250 images for testing. The resolution of the panorama is set at 128×512 in CVUSA and 256×512 in both CVACT and VIGOR-GEN. All aerial images are set to a resolution of 256×256 .

Metrics. Following previous work [15, 23, 28, 32], we adopted the widely used *Structural-Similarity (SSIM)*, *Peak Signal-to-Noise Ratio (PSNR)* and *Learned Perceptual Image Patch Similarity (LPIPS)* [40] to measure the similarity at the pixel-wise level and feature-wise level, respectively. Meanwhile, the realism of the images is measured by *Fréchet Inception Distance (FID)* [6]. Additionally, we reported the

Recall@1 (R@1) in our experiment using another cross-view image retrieval model SAIG-D [46], which indicates whether the resulting images describe the same location.

Training Details. The experiments are implemented using PyTorch. We train our model with 200 epochs using Adam [12] optimizer and $\beta_1 = 0.5, \beta_2 = 0.999$. The learning rate of the generator and discriminator is set to 0.0001 and 0.0004, respectively. For each dataset, we use the maximum possible batch size on 4 32GB NVIDIA Tesla V100 GPUs (bs=32 for CVUSA, bs=24 for CVACT, and bs=24 for VIGOR-GEN). The diversity loss is computed every 4 steps. We use DiffAug [41] {Color, Cutout} as a data augmentation strategy during the training. The $\lambda_{rec}, \lambda_{perc}$ and λ_{id} is set to 50, 50 and 10. The λ_{div} is set to 0.1 in CVUSA and CVACT, while is set to 1 in VIGOR-GEN. In previous work, the val set was considered as the test set, note that we only took the final checkpoint for testing and did not select the intermediate checkpoints.

5.2 Comparisons with state-of-the-art methods

We compared our method against several state-of-the-art methods on the CVUSA and CVACT datasets: Pix2Pix [8], XFFork [23], SelectionGAN [30], PanoGAN [35], CDE [32], S2SP [28], PPGAN [45], Sat2Density [21], ControlNet [39], Instruct pix2pix [2], and CrossViewDiff [4]. Results are shown in Table 2 and 3. As for S2SP [28], it applies the geometry project equation to calculate the projection from satellite image to street-view panorama, whose inverse process is not given in the original paper, so this method will not be compared at ground-to-aerial (g2a) generation.

Quantitative Results. In aerial-to-ground synthesis, our method demonstrates superior performance across multiple metrics on the CVUSA dataset: surpassing S2SP [28] by 6 points in SSIM and achieving improvements of 1.01 and 0.0386 in PSNR and LPIPS, respectively. Compared to the current state-of-the-art CrossViewDiff [4], our method achieves higher PSNR scores with improvements of 2.33 points on CVUSA and 2.14 points on CVACT, while also gaining a 0.0825 point improvement in SSIM on CVACT. For ground-to-aerial synthesis, our model significantly outperforms the previous best method CDE [32] in LPIPS (0.5181 vs 0.5706 on CVUSA), indicating better alignment with human visual perception. This improvement stems from our discriminator’s ability to leverage embeddings as conditions to guide generation - an advantage over CDE [32], which suffers from labeling uncertainty.

Notably, our method achieves substantial improvements in FID scores, with a 7.06-point improvement over CDE [32]. This superior performance stems from our comprehensive approach that considers both view-invariant and view-specific semantics, enhancing image realism. This advantage is particularly evident in ground-to-aerial synthesis, where other models struggle with generating obscured regions. Our method demonstrates significantly better realism on CVUSA, achieving an FID of 41.65 compared to 121.95 for baseline methods.

We further evaluate our method on the VIGOR-GEN dataset, which presents additional challenges through complex urban facades and occlusions, resulting in more complicated view-specific information. Our method achieves superior performance across all metrics on VIGOR-GEN (Table 3), setting new state-of-the-art

Table 1: Comparison of VIGOR-GEN with other existing open panorama-aerial cross-view image datasets.

Dataset	CVUSA[37]	CVACT[14]	VIGOR[44]	VIGOR-GEN
Area	field	suburban	urban	urban
Satellite resolution	750 × 750	1200 × 1200	640 × 640	640 × 640
Panorama resolution	1232 × 224	1664 × 832	2048 × 1024	2048 × 1024
Roughly centered	Yes	Yes	No	Yes
Application	Retrieval, Generation	Retrieval, Generation	Retrieval	Retrieval, Generation
#Satellite Image	44,416	44,416	90,618	103,516
#Panorama Image	44,416	44,416	105,214	103,516

Table 2: Comparison of competitive methods on CVUSA and CVACT. Note that for the FoV-only model, we follow [30] and obtain the final panorama, which consists of four street images with a FoV of 90 degrees. For fair comparison, the semantic map are discarded as an input to SelectionGAN.

Direction	Method	CVUSA					CVACT				
		SSIM↑	PSNR↑	LPIPS↓	FID↓	R@1↑	SSIM↑	PSNR↑	LPIPS↓	FID↓	R@1↑
a2g	Pix2Pix	0.2849	12.14	0.5712	82.84	0.01	0.3634	13.37	0.4943	86.21	0.00
	XFork	0.3408	13.25	0.5611	79.75	6.41	0.3701	14.17	0.4919	47.98	8.72
	SelectionGAN	0.3278	13.37	0.5331	90.72	4.58	0.4705	14.31	0.5141	95.67	6.67
	PanoGAN	0.3024	13.67	0.4684	75.24	33.11	0.4631	14.18	0.4762	82.65	28.71
	CDE	0.2980	13.87	0.4752	20.63	85.04	0.4506	13.98	0.4927	43.96	65.04
	S2SP	0.3437	13.32	0.4688	44.15	10.09	0.4521	14.14	0.4718	39.64	29.39
	PPGAN	0.3516	13.91	-	-	-	-	-	-	-	-
	Sat2Density	0.3390	14.23	-	41.43	-	0.3870	14.27	-	47.09	-
	ControlNet	0.2770	11.18	-	44.63	-	0.3400	12.15	-	47.15	-
	Instruct pix2pix	0.2550	10.66	-	68.75	-	0.3920	13.12	-	57.74	-
	CrossViewDiff	0.3710	12.00	-	23.67	-	0.4120	12.41	-	41.94	-
Ours	0.3706	14.33	0.4302	13.57	96.25	0.4945	14.55	0.4540	21.83	87.90	
g2a	Pix2Pix	0.1956	15.07	0.6220	121.95	7.85	0.0870	14.24	0.6612	133.39	13.06
	CDE	0.2167	15.19	0.5706	121.98	14.73	0.0906	14.59	0.6689	160.81	14.99
	Ours	0.2461	15.77	0.5181	41.65	95.14	0.1966	16.29	0.5551	36.54	87.81

Table 3: Comparison of existing competitive methods on our newly proposed VIGOR-GEN.

Direction	Method	VIGOR-GEN				
		SSIM↑	PSNR↑	LPIPS↓	FID↓	R@1↑
a2g	Pix2Pix[8]	0.3566	12.18	0.6114	100.25	0.01
	SelectionGAN[30]	0.3986	13.16	0.5234	104.22	7.41
	PanoGAN[35]	0.4031	13.83	0.5467	75.76	8.49
	CDE[32]	0.3672	12.72	0.6108	78.26	0.22
	S2SP[28]	0.4041	13.73	0.5422	69.28	4.54
	Ours	0.4243	13.91	0.4548	13.64	37.94
g2a	Pix2Pix[8]	0.1885	13.31	0.5876	96.26	2.41
	CDE[32]	0.1830	12.89	0.5734	95.13	3.25
	Ours	0.1901	13.99	0.5278	30.93	34.58

FID scores of 13.64 for aerial-to-ground and 30.93 for ground-to-aerial synthesis. Notably, while CDE performs well on CVUSA and CVACT, it struggles significantly on VIGOR-GEN’s urban scenes, particularly in R@1 metrics. CDE does not fit well in urban areas while our method still generates images with higher quality,

suggesting our method’s robustness in handling complex urban environments.

Qualitative Results. We provide the qualitative results of our method on different datasets to demonstrate its effectiveness. As shown in Figure 3, our method generates more realistic and detailed images with fewer artifacts compared to existing methods.

In the first group of Figure 3, our approach generates consistent and clear roads with fewer artifacts on CVACT, showcasing its ability to overcome significant visual differences. In addition, our method exhibits exceptional performance in complex scenes. For example, in the first row of the second group of Figure 3, our method synthesizes more realistic building facades, including intricate details such as windows and doors. In contrast, other methods fail to reproduce these distinctive features in panoramic views. This superior performance is attributed to our model’s consideration of both the correspondence between the source and target views and the content discrepancies between them. Unlike other models that struggle to handle view-specific semantics information differences, our method performs equally well in urban environments.

Further evidence supporting our idea is that when generating aerial-view images, other methods only produce blurred border

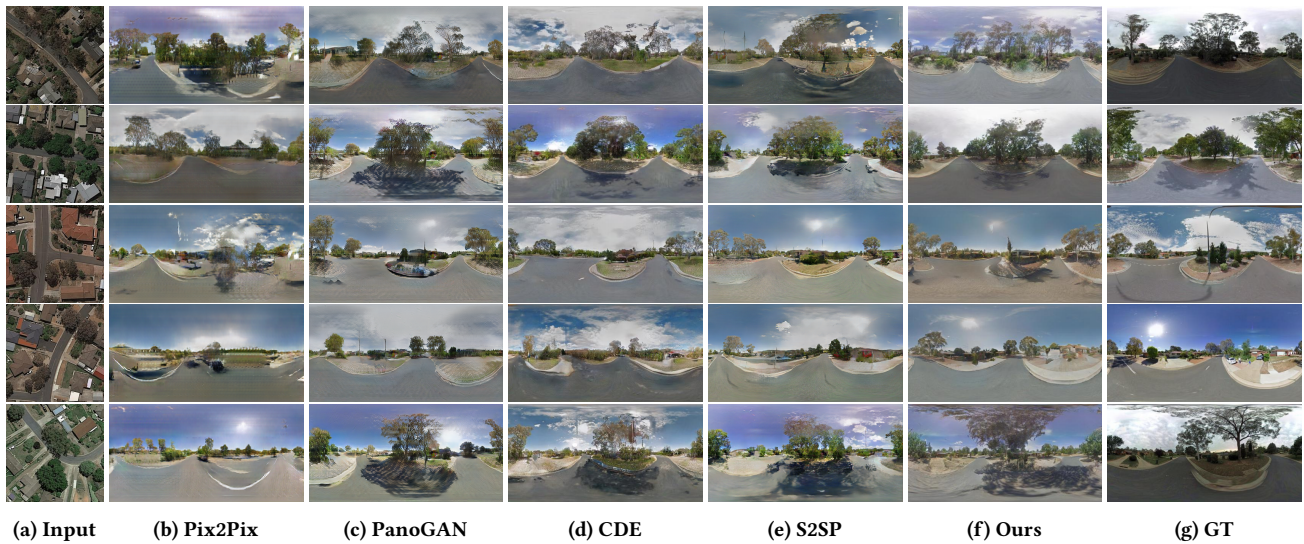


Figure 3: Comparison of current methods at a2g direction on CVACT.

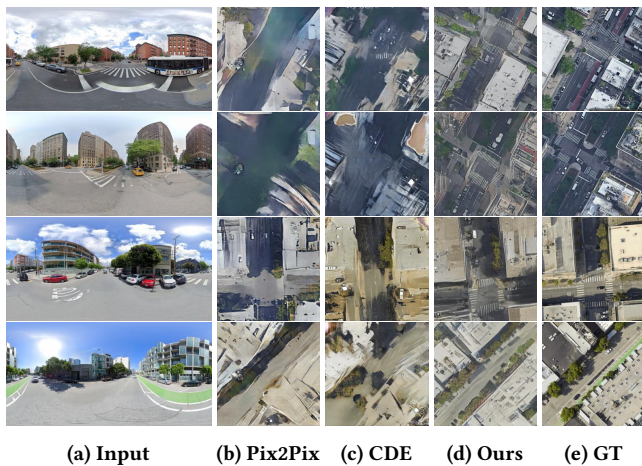


Figure 4: Comparison of g2a (ground-to-aerial) synthesis on the VIGOR-GEN dataset.

regions. As demonstrated in Figure 4, Pix2Pix [8] and CDE [32] generate central areas that are barely clear while introducing artifacts and blurs in the roof or non-central regions, where view-specific semantics aerial image information resides.

5.3 Ablation Study

In this section, we perform ablation studies to validate the effectiveness of each component in our method. We report variant models at the g2a direction on CVUSA. As the key design of our method, we first replace the retrieval embedder with a trainable pix2pix encoder (i). In this way, it is difficult for the model to transform the information from the source view to the target view, as there still exists a large domain gap.

Table 4: Ablation studies of our network on the CVUSA dataset.

Method	CVUSA				
	SSIM \uparrow	PSNR \uparrow	LPIPS \downarrow	FID \downarrow	R@1 \uparrow
Ours	0.3702	14.33	0.4302	13.57	96.25
(i)w/o Embedder	0.3312	13.66	0.4656	38.81	12.67
(ii)w/o Attn-AdaIN	0.3629	14.01	0.4461	16.51	89.42
(iii)w/o Style	0.3720	14.28	0.4412	17.88	94.23
(iv)w/o Ret.	0.3571	13.75	0.4377	15.74	87.67
(v)Same Structure	0.3490	14.06	0.4332	14.29	96.12
(vi)w/o coarse D	0.3454	14.11	0.4308	13.67	95.61

The second experiment removes the attn-AdaIN in our model (ii). Without this component, the model loses the capability to fuse the retrieval embedding into the corresponding semantic regions effectively, which leads to a decrease in similarity.

Next, we also analyze the roles of the style (iii) and retrieval embedding (iv) in our generator. The fusion of retrieved information and style improves the network from two perspectives: correspondence and diversity. By fusing the retrieved information and style, we improve the model from two key retrieval-related perspectives: correspondence and diversity. First, by fusing embeddings in deep layers, the model ensures the generation of semantically consistent representations in the target view against the visual difference. This improves cross-view retrieval performance by aligning the target image more closely with the source view. We observe a degradation of the performance in various metrics from Table 4, especially in R@1 (with 9% drop). Second, the additional style information promotes the diversity of visual features and enriches the visual representations, which facilitates the generation of view-specific semantics information in the target view. This is crucial for generating distinct images in retrieval tasks, where diversity in output is essential for improving retrieval accuracy. However,

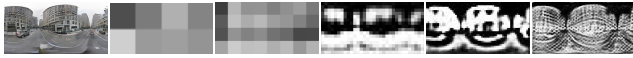


Figure 5: Visualization of the weight map M on VIGOR-GEN.

Table 5: Comparison of different Embedders in our generator on CVUSA at a2g.

Embedder	CVUSA				
	SSIM \uparrow	PSNR \uparrow	LPIPS \downarrow	FID \downarrow	R@1 \uparrow
SAIG	0.3706	14.32	0.4302	13.57	96.25
LPN	0.3559	13.89	0.4544	25.29	30.45

while this integration results in a slight increase in SSIM, it leads to significant declines in LPIPS and FID scores. We further investigate the impact of different structural designs. If the model uses the same structure (i.e., ResBlock-S) to generate structural and facade information, metrics such as FID and LPIPS rise. Besides, the performance of the model degrades if the discriminator for coarse images is disabled. Consequently, facade generation modules reinforce the performance of the network in cross-view synthesis.

Finally, to better understand the contribution of attn-AdaIN, we visualize the mask M learned on different feature levels in Figure 5, where the brighter pixel indicates the higher weight for retrieval embedding. This highlights the role of the retrieval embedding in guiding the generation process by focusing on relevant features, which is crucial for successful information retrieval.

5.4 Further Discussion

The retrieval embedder bridges the domain gap and provides a stable direction of gradient descent. By using retrieval loss, the embedding space remains smooth, aiding in better cross-view retrieval. Specifically, when the model generates an incorrect target image identity, the retrieval loss-guided embedding offers an optimal gradient direction for the generator to correct the identity. In contrast, embedders trained for discriminative tasks may produce non-smooth embedding spaces. For example, we compare the use of LPN [34] in the generator, which treats cross-view image retrieval as a classification task and applies instance loss [42]. As shown in Table 5, the generator using LPN [34] performs significantly worse than the generator using SAIG, highlighting the superiority of retrieval loss-based embedding.

Model Size. Table 6 compares our model with state-of-the-art methods in terms of model size (Params), inference speed (FPS), and generation quality (FID). Our model achieves the smallest size (25.9M), significantly smaller than others like SelectionGAN (58.3M) and PanoGAN (88.0M), making it lightweight and easier to deploy. Additionally, it also achieves the highest inference speed (39.2 FPS), far surpassing methods like SelectionGAN (18.0 FPS) and PanoGAN (19.1 FPS), demonstrating its suitability for real-time applications. Most importantly, our model achieves the best generation quality with an FID score of 13.57, significantly outperforming competitors like CDE (20.63) and S2SP (44.15). These results highlight the effectiveness of our lightweight design and optimized architecture, balancing efficiency and performance for practical applications.

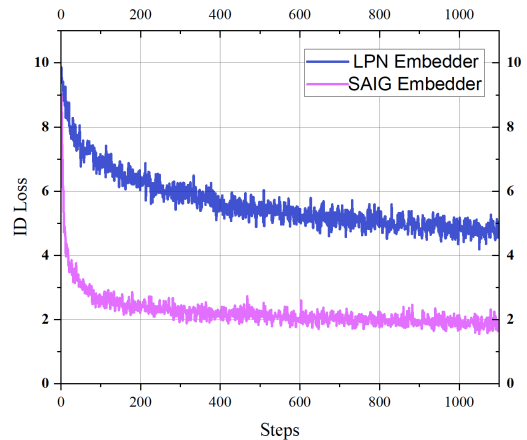


Figure 6: The curve of ID loss in generator using different embedders.

Loss. The experiment investigates the impact of different embedders on the generator’s performance and convergence, particularly comparing the SAIG embedder with the LPN embedder. The LPN embedder, as introduced in [34], treats cross-view image retrieval as a classification problem and employs instance loss [42] for training. However, this approach leads to a non-smooth embedding space, which negatively affects the generator’s performance and convergence speed. As shown in Table 5, the generator with the SAIG embedder outperforms the LPN embedder across all metrics, including SSIM, PSNR, LPIPS, FID, and R@1, indicating superior generation quality and domain adaptation. Additionally, figure 6 illustrates that the ID loss of the generator converges more rapidly and stably with the SAIG embedder compared to the LPN embedder, further highlighting the advantages of the retrieval-based embedding strategy in achieving smoother and more effective optimization.

Different Residual Block. Based on the experimental results shown in Figure 7, it can be observed that models using only Structure-S generate images with visible artifacts, such as texture inconsistencies and less realistic details, particularly in complex scenarios like dense vegetation or architectural features. In contrast, the combination of Structure-S and Structure-T leads to substantial improvements, producing images that are smoother, more coherent, and closer to the ground truth. The Structure-S block captures global structural information effectively, while the addition of Structure-T enhances local detail modeling, balancing the global and local features. This combination results in sharper object contours, improved texture quality, and an overall more realistic appearance. These findings validate the benefits of combining both residual blocks and align with the ablation studies, demonstrating superior image quality and structural accuracy.

Higher Quality. To showcase the superior capability of our model, we conduct experiments on high-resolution cross-view image synthesis at 256×1024 resolution. As shown in Table 7, our method outperforms existing state-of-the-art approaches, including SelectionGAN [30] and PanoGAN [35], across all evaluation metrics. Specifically, our model achieves significant improvements in SSIM,

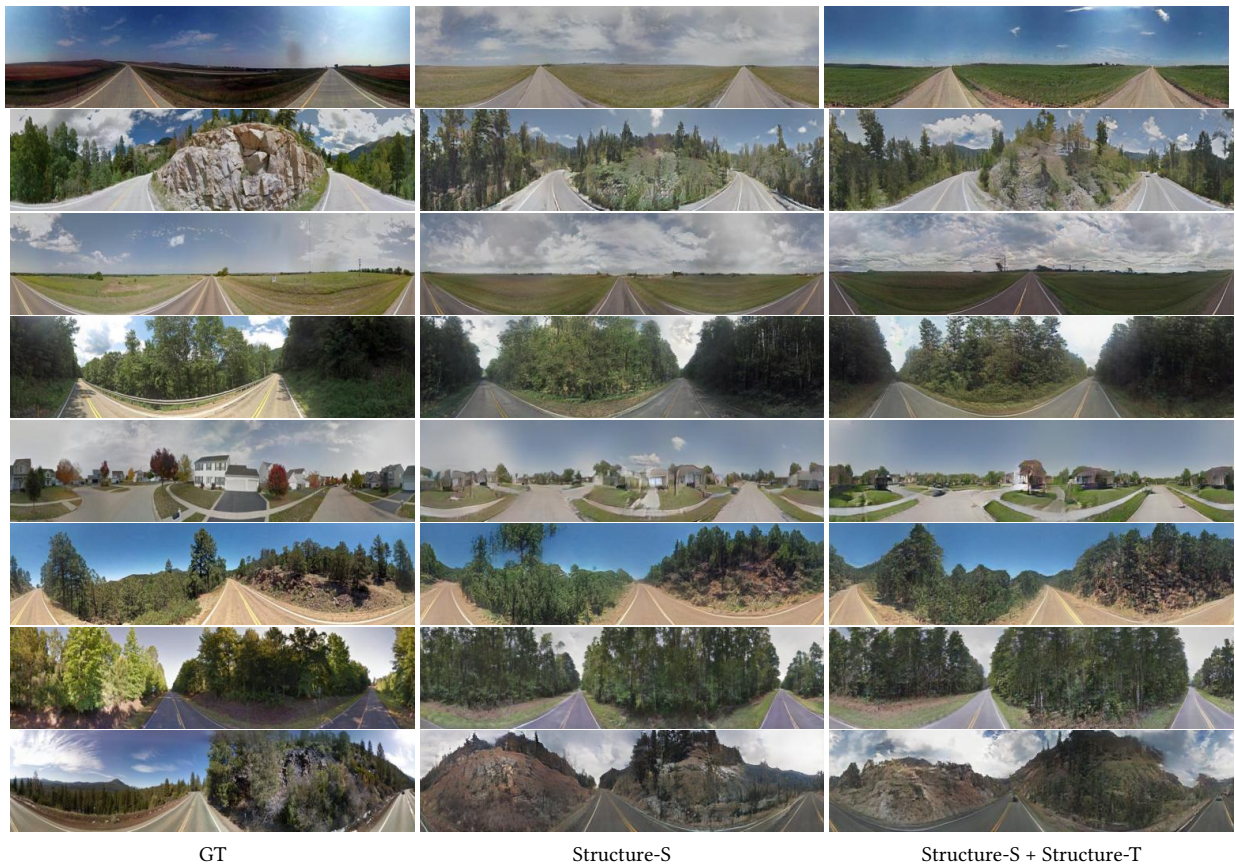


Figure 7: Comparison of images generated by models using different Residual Blocks.

Table 6: Comparison of model size for different model.

Model	#Params	FPS	FID
Pix2Pix	41.8M	34.1	82.84
XFork	39.2M	33.8	79.75
SelectionGAN	58.3M	18.0	90.72
PanoGAN	88.0M	19.1	75.24
CDE	37.3M	35.9	20.63
S2SP	33.6M	22.1	44.15
Ours	25.9M	39.2	13.57

Table 7: Comparison of our generator with different methods on CVUSA at 256×1024 .

Dataset	Method	SSIM \uparrow	PSNR \uparrow	LPIPS \downarrow	FID \downarrow	R@1 \uparrow
CVUSA	SelectionGAN	0.4010	13.21	0.6169	103.27	3.81
	PanoGAN	0.3575	13.47	0.5566	81.91	30.58
	Ours	0.4232	14.11	0.4978	17.88	96.01
CVACT	SelectionGAN	0.4876	14.28	0.5232	97.63	5.76
	PanoGAN	0.4915	14.31	0.4959	86.61	23.02
	Ours	0.5513	14.48	0.4938	24.62	86.91
VIGOR-GEN	SelectionGAN	0.4154	13.11	0.5225	106.24	7.80
	PanoGAN	0.4229	13.68	0.4933	79.72	8.26
	Ours	0.4771	14.01	0.4876	23.54	36.18

PSNR, LPIPS, FID, and R@1. The improved retrieval accuracy highlights our model’s ability to generate images that are more consistent and relevant in the context of cross-view image retrieval. The enhanced retrieval accuracy underscores our model’s ability to generate images that are not only structurally consistent but also contextually relevant for cross-view image retrieval. These results demonstrate our approach excels in producing high-quality images with improved structural consistency and perceptual fidelity.

6 Conclusion

In this work, we present a retrieval-guided approach for cross-view image synthesis, leveraging information retrieval techniques to bridge the domain gap in challenging cross-view tasks. By incorporating a retrieval network as the embedder, our framework effectively captures view-invariant and view-specific semantics, enabling accurate cross-view correspondence modeling without the need for auxiliary data. Additionally, we introduce novel generators that enhance the synthesis of both structure and facade, improving the generation of view-specific details in the target image. To facilitate model evaluation in real-world scenarios, we also introduce VIGOR-GEN, a large-scale, urban-focused dataset. Extensive experiments on CVUSA, CVACT, and VIGOR-GEN confirm the effectiveness of our method, achieving state-of-the-art performance across multiple evaluation metrics, including SSIM and FID. Our

work successfully bridges the gap between information retrieval and image synthesis, offering valuable insights into how retrieval techniques can drive improvements in complex cross-domain generation tasks.

References

- [1] Benjamin Bischke, Damian Borth, Christian Schulze, and Andreas Dengel. 2016. Contextual enrichment of remote-sensed events with social media streams. In *Proceedings of the 24th ACM international conference on Multimedia*. 1077–1081.
- [2] Tim Brooks, Aleksander Holynski, and Alexei A Efros. 2023. Instructpix2pix: Learning to follow image editing instructions. In *Proceedings of the IEEE/CVF Conference on Computer Vision and Pattern Recognition*. 18392–18402.
- [3] Yunjey Choi, Youngjung Uh, Jaejun Yoo, and Jung-Woo Ha. 2020. Stargan v2: Diverse image synthesis for multiple domains. In *Proceedings of the IEEE/CVF conference on computer vision and pattern recognition*. 8188–8197.
- [4] Florinel-Alin Croitoru, Vlad Hondru, Radu Tudor Ionescu, and Mubarak Shah. 2023. Diffusion models in vision: A survey. *IEEE Transactions on Pattern Analysis and Machine Intelligence* (2023).
- [5] Harm De Vries, Florian Strub, Jérémie Mary, Hugo Larochelle, Olivier Pietquin, and Aaron C Courville. 2017. Modulating early visual processing by language. *Advances in Neural Information Processing Systems* 30 (2017).
- [6] Martin Heusel, Hubert Ramsauer, Thomas Unterthiner, Bernhard Nessler, and Sepp Hochreiter. 2017. Gans trained by a two time-scale update rule converge to a local nash equilibrium. *Advances in neural information processing systems* 30 (2017).
- [7] Xun Huang and Serge Belongie. 2017. Arbitrary style transfer in real-time with adaptive instance normalization. In *Proceedings of the IEEE international conference on computer vision*. 1501–1510.
- [8] Phillip Isola, Jun-Yan Zhu, Tinghui Zhou, and Alexei A Efros. 2017. Image-to-image translation with conditional adversarial networks. In *Proceedings of the IEEE conference on computer vision and pattern recognition*. 1125–1134.
- [9] Tero Karras, Miika Aittala, Janne Hellsten, Samuli Laine, Jaakko Lehtinen, and Timo Aila. 2020. Training generative adversarial networks with limited data. *Advances in neural information processing systems* 33 (2020), 12104–12114.
- [10] Tero Karras, Samuli Laine, and Timo Aila. 2019. A style-based generator architecture for generative adversarial networks. In *Proceedings of the IEEE/CVF conference on computer vision and pattern recognition*. 4401–4410.
- [11] Tero Karras, Samuli Laine, Miika Aittala, Janne Hellsten, Jaakko Lehtinen, and Timo Aila. 2020. Analyzing and improving the image quality of stylegan. In *Proceedings of the IEEE/CVF conference on computer vision and pattern recognition*. 8110–8119.
- [12] Diederik P Kingma and Jimmy Ba. 2014. Adam: A method for stochastic optimization. *arXiv preprint arXiv:1412.6980* (2014).
- [13] Hsin-Ying Lee, Hung-Yu Tseng, Qi Mao, Jia-Bin Huang, Yu-Ding Lu, Maneesh Singh, and Ming-Hsuan Yang. 2020. Dri++: Diverse image-to-image translation via disentangled representations. *International Journal of Computer Vision* 128 (2020), 2402–2417.
- [14] Liu Liu and Hongdong Li. 2019. Lending orientation to neural networks for cross-view geo-localization. In *Proceedings of the IEEE/CVF conference on computer vision and pattern recognition*. 5624–5633.
- [15] Xiaohu Lu, Zuoyue Li, Zhaopeng Cui, Martin R Oswald, Marc Pollefeys, and Rongjun Qin. 2020. Geometry-aware satellite-to-ground image synthesis for urban areas. In *Proceedings of the IEEE/CVF Conference on Computer Vision and Pattern Recognition*. 859–867.
- [16] Jisan Mahmud, True Price, Akash Bapat, and Jan-Michael Frahm. 2020. Boundary-aware 3D building reconstruction from a single overhead image. In *Proceedings of the IEEE/CVF Conference on Computer Vision and Pattern Recognition*. 441–451.
- [17] Qi Mao, Hsin-Ying Lee, Hung-Yu Tseng, Siwei Ma, and Ming-Hsuan Yang. 2019. Mode seeking generative adversarial networks for diverse image synthesis. In *Proceedings of the IEEE/CVF conference on computer vision and pattern recognition*. 1429–1437.
- [18] Gellért Mátyus, Wenjie Luo, and Raquel Urtasun. 2017. Deeproadmapper: Extracting road topology from aerial images. In *Proceedings of the IEEE international conference on computer vision*. 3438–3446.
- [19] Takeru Miyato, Toshiki Kataoka, Masanori Koyama, and Yuichi Yoshida. 2018. Spectral normalization for generative adversarial networks. *arXiv preprint arXiv:1802.05957* (2018).
- [20] Taesung Park, Ming-Yu Liu, Ting-Chun Wang, and Jun-Yan Zhu. 2019. Semantic image synthesis with spatially-adaptive normalization. In *Proceedings of the IEEE/CVF conference on computer vision and pattern recognition*. 2337–2346.
- [21] Ming Qian, Jincheng Xiong, Gui-Song Xia, and Nan Xue. 2023. Sat2density: Faithful density learning from satellite-ground image pairs. In *Proceedings of the IEEE/CVF International Conference on Computer Vision*. 3683–3692.
- [22] Aditya Ramesh, Prafulla Dhariwal, Alex Nichol, Casey Chu, and Mark Chen. 2022. Hierarchical text-conditional image generation with clip latents. *arXiv preprint arXiv:2204.06125* 1, 2 (2022), 3.
- [23] Krishna Regmi and Ali Borji. 2018. Cross-view image synthesis using conditional gans. In *Proceedings of the IEEE conference on Computer Vision and Pattern Recognition*. 3501–3510.
- [24] Elad Richardson, Yuval Alaluf, Or Patashnik, Yotam Nitzan, Yaniv Azar, Stav Shapiro, and Daniel Cohen-Or. 2021. Encoding in style: a stylegan encoder for image-to-image translation. In *Proceedings of the IEEE/CVF conference on computer vision and pattern recognition*. 2287–2296.
- [25] Robin Rombach, Andreas Blattmann, Dominik Lorenz, Patrick Esser, and Björn Ommer. 2022. High-resolution image synthesis with latent diffusion models. In *Proceedings of the IEEE/CVF conference on computer vision and pattern recognition*. 10684–10695.
- [26] Chitwan Saharia, William Chan, Saurabh Saxena, Lala Li, Jay Whang, Emily L Denton, Kamyar Ghasemipour, Raphael Gontijo Lopes, Burcu Karagol Ayan, Tim Salimans, et al. 2022. Photorealistic text-to-image diffusion models with deep language understanding. *Advances in Neural Information Processing Systems* 35 (2022), 36479–36494.
- [27] Axel Sauer, Tero Karras, Samuli Laine, Andreas Geiger, and Timo Aila. 2023. Stylegan-t: Unlocking the power of gans for fast large-scale text-to-image synthesis. *arXiv preprint arXiv:2301.09515* (2023).
- [28] Yujiao Shi, Dylan Campbell, Xin Yu, and Hongdong Li. 2022. Geometry-Guided Street-View Panorama Synthesis From Satellite Imagery. *IEEE Transactions on Pattern Analysis and Machine Intelligence* 44, 12 (2022), 10009–10022. doi:10.1109/TPAMI.2022.3140750
- [29] Yujiao Shi, Liu Liu, Xin Yu, and Hongdong Li. 2019. Spatial-aware feature aggregation for image based cross-view geo-localization. *Advances in Neural Information Processing Systems* 32 (2019).
- [30] Hao Tang, Dan Xu, Nicu Sebe, Yanzhi Wang, Jason J Corso, and Yan Yan. 2019. Multi-channel attention selection gan with cascaded semantic guidance for cross-view image translation. In *Proceedings of the IEEE/CVF conference on computer vision and pattern recognition*. 2417–2426.
- [31] Ming Tao, Hao Tang, Fei Wu, Xiao-Yuan Jing, Bing-Kun Bao, and Changsheng Xu. 2022. Df-gan: A simple and effective baseline for text-to-image synthesis. In *Proceedings of the IEEE/CVF Conference on Computer Vision and Pattern Recognition*. 16515–16525.
- [32] Aysim Toker, Qunjie Zhou, Maxim Maximov, and Laura Leal-Taixé. 2021. Coming down to earth: Satellite-to-street view synthesis for geo-localization. In *Proceedings of the IEEE/CVF Conference on Computer Vision and Pattern Recognition*. 6488–6497.
- [33] Hugo Touvron, Matthieu Cord, Alexandre Sablayrolles, Gabriel Synnaeve, and Hervé Jégou. 2021. Going deeper with image transformers. In *Proceedings of the IEEE/CVF international conference on computer vision*. 32–42.
- [34] Tingyu Wang, Zhedong Zheng, Chenggang Yan, Jiyong Zhang, Yaoqi Sun, Bolun Zheng, and Yi Yang. 2021. Each part matters: Local patterns facilitate cross-view geo-localization. *TCSVT* (2021).
- [35] Songsong Wu, Hao Tang, Xiao-Yuan Jing, Haifeng Zhao, Jianjun Qian, Nicu Sebe, and Yan Yan. 2022. Cross-view panorama image synthesis. *IEEE Transactions on Multimedia* (2022).
- [36] Shuai Yang, Liming Jiang, Ziwei Liu, and Chen Change Loy. 2022. Pastiche master: Exemplar-based high-resolution portrait style transfer. In *Proceedings of the IEEE/CVF Conference on Computer Vision and Pattern Recognition*. 7693–7702.
- [37] Menghua Zhai, Zachary Bessinger, Scott Workman, and Nathan Jacobs. 2017. Predicting ground-level scene layout from aerial imagery. In *Proceedings of the IEEE Conference on Computer Vision and Pattern Recognition*. 867–875.
- [38] Menghua Zhai, Zachary Bessinger, Scott Workman, and Nathan Jacobs. 2017. Predicting ground-level scene layout from aerial imagery. In *CVPR*. 867–875.
- [39] Lvmin Zhang, Anyi Rao, and Maneesh Agrawala. 2023. Adding conditional control to text-to-image diffusion models. In *Proceedings of the IEEE/CVF International Conference on Computer Vision*. 3836–3847.
- [40] Richard Zhang, Phillip Isola, Alexei A Efros, Eli Shechtman, and Oliver Wang. 2018. The unreasonable effectiveness of deep features as a perceptual metric. In *Proceedings of the IEEE conference on computer vision and pattern recognition*. 586–595.
- [41] Shengyu Zhao, Zhijian Liu, Ji Lin, Jun-Yan Zhu, and Song Han. 2020. Differentiable augmentation for data-efficient gan training. *Advances in Neural Information Processing Systems* 33 (2020), 7559–7570.
- [42] Zhedong Zheng, Yunchao Wei, and Yi Yang. 2020. University-1652: A multi-view multi-source benchmark for drone-based geo-localization. In *Proceedings of the 28th ACM international conference on Multimedia*. 1395–1403.
- [43] Peihao Zhu, Rameen Abdal, Yipeng Qin, and Peter Wonka. 2020. Sean: Image synthesis with semantic region-adaptive normalization. In *Proceedings of the IEEE/CVF Conference on Computer Vision and Pattern Recognition*. 5104–5113.
- [44] Sijie Zhu, Taojiannan Yang, and Chen Chen. 2021. Vigor: Cross-view image geo-localization beyond one-to-one retrieval. In *Proceedings of the IEEE/CVF Conference on Computer Vision and Pattern Recognition*. 3640–3649.
- [45] Yingying Zhu, Shihai Chen, Xiufan Lu, and Jianyong Chen. 2023. Cross-view Image Synthesis from a Single Image with Progressive Parallel GAN. *IEEE Transactions on Geoscience and Remote Sensing* (2023).

[46] Yingying Zhu, Hongji Yang, Yuxin Lu, and Qiang Huang. 2023. Simple, Effective and General: A New Backbone for Cross-view Image Geo-localization. *arXiv*

e-prints, Article arXiv:2302.01572 (Feb. 2023), arXiv:2302.01572 pages. doi:10.48550/arXiv.2302.01572 arXiv:2302.01572 [cs.CV]